

Fast Security-Constrained Optimal Power Flow through Low-Impact and Redundancy Screening

Richard Weinhold, Robert Mieth

Abstract—Network-constrained dispatch decisions are not only restricted by the thermal limits of the power lines, but also by complex security requirements related to contingency scenarios, e.g. the N-1-criterion. For real-world networks, the security-constrained optimal power flow (SCOPF) leads to a prohibitive increase in complexity even for linearized (DC) power flow equations. This paper presents a set of methods for fast, yet exact, SCOPF computation by reducing the power flow and contingency constraints to a minimal subset. The constraint reduction is performed by an iterative algorithm with performance guarantees based on both general algebraic theory and exploiting peculiarities of the optimal dispatch problem. The method is showcased on the classic IEEE 118-bus test system and on a full-scale real-world system. The numerical experiments rely on open-source software and data and our implementation is published supplementary to the paper.

NOMENCLATURE

A. Sets

\mathcal{C}	Set of contingency scenarios with $C = \mathcal{C} $
$\mathcal{F}(B, \bar{f})$	Feasible region of system (B, \bar{f})
\mathcal{G}	Set of generators with $G = \mathcal{G} $
\mathcal{I}, \mathcal{J}	Set of indices
\mathcal{L}	Set of lines/edges with $L = \mathcal{L} $
\mathcal{L}_n	Set of lines connected to node n , $\mathcal{L}_n \subseteq \mathcal{L}$
\mathcal{N}	Set of nodes with $N = \mathcal{N} $
\mathcal{T}	Set of time steps indexed with $T = \mathcal{T} $

B. Parameters and Variables

d_t	Active power demand at t indexed by $d_{t,n}, n \in \mathcal{N}$
f_t	Active power flow at t indexed by $f_{t,l}, l \in \mathcal{L}$
\bar{f}	Maximum line capacity indexed by $\bar{f}_l, l \in \mathcal{L}$
g_t	Active power generation at t indexed by $g_{t,i}, i \in \mathcal{G}$
\underline{g}_t	Lower generation limit at t indexed by $\underline{g}_{t,i}, i \in \mathcal{G}$
\bar{g}_t	Upper generation limit at t indexed by $\bar{g}_{t,i}, i \in \mathcal{G}$
x_t	Nodal injection at t indexed by $x_{t,n}, n \in \mathcal{N}$
\tilde{x}, \hat{x}	Asymmetric bounds on nodal injection
\underline{x}, \bar{x}	Symmetric bounds on nodal injection
B	Generalized power transfer distribution matrix
I	Identity matrix of appropriate dimensions
LODF_{lc}	Line outage distribution factor for line l under c
M	Mapping of generators to nodes
η	Impact screening margin

C. Operators

$ \mathcal{X} $	Cardinality of set \mathcal{X}
\mathcal{X}°	Interior of set \mathcal{X}
X^\top	Transpose of matrix X
X_i	Row vector equal to the i -th row of X
X_{ij}	j -th entry in the i -th row of X

I. INTRODUCTION

Power flow physics and transmission limits constrain electricity market transactions. With increasing uncertainty, mainly driven by the proliferation of intermittent renewable genera-

tion, a precise calculation of securely available transmission capacity can improve market efficiency and system reliability, [1]. For example, in May 2015 the transmission system operators (TSOs) of central western Europe (CWE) inaugurated flow based market coupling (FBMC) to replace net transfer capacities as cross-border trading constraints. FBMC includes constraints imposed by critical network elements and outage scenarios (contingencies), so called critical branches under critical outages (CBCOs), [2], into its market clearing algorithm, thus “*bringing commercial transactions closer to the physical reality*”, [3]. As a result, TSOs were able to effectively increase the system’s overall transfer capacity leading to an improvement in distribution of renewable generation and price convergence between the CWE market zones, [2], [3].

The identification of those CBCOs and power flow analyses with contingency scenarios in general is commonly addressed by security-constrained optimal power flow (SCOPF), [4]. However, given the large scale of real-world power systems and the resulting number of possible contingencies, obtaining a practical SCOPF is often obstructed by the dimensions of the resulting numerical problem and its computational complexity. While TSOs are primarily concerned with detailed real-time solutions, economists and market analysts, on the other hand, require robust and interpretable methods that can accommodate time horizons of weeks, months or years, [5]. This paper proposes a method to identify a minimal set of constraints that exactly represents the solution space of the SCOPF problem, thus significantly reducing the computational effort and enabling multiperiod market simulations that truly internalize secure physical network constraints.

The efficient selection of relevant contingencies is the central theme of classic and recent approaches to accelerate SCOPF computation, [6]–[14]. An established iterative method, e.g. [6], [7], [10], [12], solves a reduced base problem and then tests the obtained solution for possible violation of constraints inferred by contingencies that have not been considered in the previous solution. If violations are detected, the problem is solved again including those constraints and the procedure restarts. The selection and order of constraints to be tested can be decided, for instance, based on line loading, [6], impact bounds, [8], or a ranking of corrective actions, [11].

An alternative approach looks for (steady-state) security regions, [13], [15], i.e. a feasible set of nodal injection vectors for which all imposed security constraints are satisfied. Identifying or creating constraints that imply the satisfaction of other constraints, e.g. [9], [10], [16]–[18], can point towards constraints that have no impact on the problem solution and, thus, can be dropped. In [9], [10] contingencies and their related constraints are dropped if there exist *dominant* contingencies that cause more severe violation of the remaining constraints. The authors of [17] define bounds on the decision

variables of a security constrained unit commitment (SCUC) problem and then identify constraints that are redundant given those bounds. Similarly, [18] employs a relaxation technique to define and identify constraints that do not influence the feasible region of the problem, i.e. that are inactive.

The constraint sets studied in approaches [6]–[13] depend on a specific SCOPF solution, i.e. a specific set of input parameters (e.g. demand vectors) or objective functions. Alternatively, [14], [19], [20] propose the notion of *umbrella contingencies*. This contingency (sub)set contains the most restrictive outages that cover for all other possible outages implicitly and is independent of the structure of the objective or additional constraints. Solving the SCOPF with this subset of contingencies, has been shown to significantly reduce the calculation time, but identifying this set still poses some challenges. Network partitioning to enable parallel computation, [14], and approximate pre-processing, [19], has been proposed to improve umbrella constraint discovery. However, these approaches require an additional layer of implementation and the results are sensitive to the partitioning method. In [20] neural networks are proposed to predict umbrella constraints if system conditions change, but this requires previous identification of training sets.

This paper proposes a new set of methods to improve the computational tractability of SCOPF problems by identifying and removing redundant constraints. The main contributions are as follows:

- 1) Similar to [14], [19] we propose a method to identify a minimal set of *essential* constraints that exactly represents the feasible region of the SCOPF. However, relative to [14], [19] we improve the discovery of essential constraints by leveraging a geometric algorithm based on [21] that avoids additional preprocessing and robustly scales towards large real-world systems.
- 2) We propose the notion of *conditional essential* constraints to further reduce the set of constraints. These constraints are essential under the condition that the nodal injection at each node does not exceed predefined limits.
- 3) We show that computational complexity can be further reduced by ignoring the impact of contingencies on line flows below a certain threshold. We show that this approach relates directly to the common operational practice of security margins and discuss the threshold choice.
- 4) The proposed methods have been implemented in an open-source framework that readily supports input from MatPower and Open-Power-System-Data and can be downloaded from [22].

II. PROBLEM FORMULATION

In this paper we consider a preventive SCOPF problem on multiple time steps $t \in \mathcal{T}$. As common for this type of analyses we leverage the DC power flow approximation, [4], [14], to derive a linear relationship between nodal active power injections, contingencies and line flows.

A. Power Flow Preliminaries

The physical network is represented by the set of nodes \mathcal{N} with $N = |\mathcal{N}|$, the set of generators \mathcal{G} with $G = |\mathcal{G}|$ and the set of lines \mathcal{L} with $L = |\mathcal{L}|$. Vector g_t indexed by $g_{t,i} \geq 0$

denotes the active power generation of each generator i and vector d_t indexed by $d_{t,n} \leq 0$ denotes the aggregated active demand at each node $n \in \mathcal{N}$ at time t . At every time t the vector of nodal injections is given by

$$x_t = d_t + Mg_t \quad (1)$$

indexed by $x_{t,n}$ where M is a mapping of generators to nodes. Upper and lower generation limits are given by \bar{g}_t and \underline{g}_t indexed by $\bar{g}_{t,i}$ and $\underline{g}_{t,i}$ respectively. Each line $l \in \mathcal{L}$ is a directed connection with arbitrary but fixed orientation between one sending node s and one receiving node r . At each time t positive flow $f_{t,l} \geq 0$ indicates active power flow from s to r and negative flow $f_{t,l} \leq 0$ indicates active power flow from r to s over line l . For all $l \in \mathcal{L}$ the power flows are collected in the vector f_t indexed by $f_{t,l}$ and the line capacities are given by vector \bar{f} indexed by \bar{f}_l . The physical power flow equations are approximated by power transfer distribution factors (PTDFs) where the PTDF matrix $B^0 \in \mathbb{R}^{L \times N}$ is a linear mapping of nodal injections x_t to power flows f_t such that:

$$f_t = B^0 x_t. \quad (2)$$

We refer the interested reader to Appendix A for a derivation of the PTDF matrix. Superscript 0 denotes the base-case PTDF, i.e. the pre-contingency (N-0) case without any outages.

B. Contingency Preliminaries

Consider a contingency scenario c such that $c \subseteq \mathcal{L}$ is the set of one or multiple lines that experience an unplanned outage. The post-contingency flow along any line $l \notin c$ is determined by line outage distribution factor $\text{LODF}_{lc} \in \mathbb{R}$ such that:

$$f_{t,l}^c = f_{t,l}^0 + \text{LODF}_{lc} f_{t,c}^0, \quad (3)$$

where $f_{t,l}^c$ is the flow on line l in outage scenario c , and $f_{t,l}^0$ is the pre-contingency flow on line l and $f_{t,c}^0$ is the vector of pre-contingency line flows of lines c at time t . Note that LODF_{lc} can be either positive or negative. For the derivations of the LODFs we refer the interested reader to Appendix B. For every possible contingency $c \in \mathcal{C}$ indexed by $c = \{1, \dots, C\}$ we use these sensitivity factors to define contingency-PTDF matrices B^c as:

$$B^c = B^0 + \begin{bmatrix} \text{LODF}_{1c} B_c^0 \\ \text{LODF}_{2c} B_c^0 \\ \vdots \\ \text{LODF}_{Lc} B_c^0 \end{bmatrix}, \quad \forall c \in \mathcal{C}, \quad (4)$$

where B_c^0 is the $L \times |c|$ matrix collecting the rows of B^0 corresponding to the outages in c . Given a vector of nodal injections x_t the resulting post-contingency power flows after outage c can be computed as:

$$f_t^c = B^c x_t. \quad (5)$$

Remark 1. Other types of contingencies, e.g. generator outages, allow similar representations in terms of line flow sensitivities, [17], and the formulations and methodology proposed in this paper can be extended to accommodate them.

C. Security Constrained Optimal Power Flow

We consider a multi-period preventive OPF problem given by:

$$\min_{g,x} \sum_{t \in \mathcal{T}} C(g_t) \quad (6a)$$

$$\text{s.t.} \quad d_t + Mg_t = x_t \quad \forall t \in \mathcal{T} \quad (6b)$$

$$e^\top x_t = 0 \quad \forall t \in \mathcal{T} \quad (6c)$$

$$g_t \leq g_t \leq \bar{g}_t \quad \forall t \in \mathcal{T} \quad (6d)$$

$$-\bar{f}^0 \leq B^0 x_t \leq \bar{f}^0 \quad \forall t \in \mathcal{T} \quad (6e)$$

$$-\bar{f}^c \leq B^c x_t \leq \bar{f}^c \quad \forall t \in \mathcal{T}, \forall c \in \mathcal{C}. \quad (6f)$$

Objective (6a) minimizes the cost of generation given by cost-function $C(g_t)$. Eqs. (6b) and (6c) enforce the nodal and global energy balances. Eq. (6d) imposes limits on the active power output of the generators. Eqs. (6e) and (6f) enforce that no line is overloaded due to the resulting power flow for the base case and every contingency. Thus, (6e) and (6f) define the feasible region of nodal injections given base and contingency PTDFs, and the thermal line flow limits is given as:

$$\mathcal{F}(B, \bar{f}) = \{x : -\bar{f} \leq Bx \leq \bar{f}\}, \quad (7)$$

where

$$B = \begin{bmatrix} B^0 \\ B^1 \\ \vdots \\ B^C \end{bmatrix}, \quad \bar{f} = \begin{bmatrix} \bar{f}^0 \\ \bar{f}^1 \\ \vdots \\ \bar{f}^C \end{bmatrix}. \quad (8)$$

Using (7), (8) the following formulation is equivalent to (6):

$$\min \sum_{t \in \mathcal{T}} C(g_t) \quad (9a)$$

$$\text{s.t.} \quad (6b) \text{--}(6d) \quad (9b)$$

$$x_t \in \mathcal{F}(B, \bar{f}) \quad \forall t \in \mathcal{T}. \quad (9c)$$

Note that (9) can be extended to accommodate more complex problems, e.g. security constrained unit commitment, *without* changing (9c).

To reflect the upper and lower bounds of feasible region $\mathcal{F}(B, \bar{f})$, each PTDF matrix B^0, \dots, B^C introduces $2L$ linear inequalities to the problem. Thus, even the least complex set of $N-1$ contingencies, i.e. only one simultaneous outage, requires $2L(L+1)$ inequalities to define feasible region $\mathcal{F}(B, \bar{f})$. Furthermore, this set of inequalities has to be evaluated for every time step t to solve (6). Therefore, the resulting problem size quickly becomes computationally intractable with increasing system size and more complex contingency scenarios. However, it has been shown that only a subset of these inequalities is necessary to sufficiently define $\mathcal{F}(B, \bar{f})$, [10], [14], thus reducing computational complexity. In the following section we propose a procedure that efficiently discovers the minimal set of inequalities based on endogenous model parameters and exogenous data characteristics.

III. REDUNDANCY SCREENING

We consider the set of feasible solutions (feasible region) $\mathcal{F}(B, \bar{f})$ to a linear program (LP) defined by system $(B \in \mathbb{R}^{M \times N}, \bar{f} \in \mathbb{R}^M)$ with $M > N$ and set of indices \mathcal{I} such that:

$$\mathcal{F}(B, \bar{f}, \mathcal{I}) = \{x \in \mathbb{R}^N : B_i x \leq \bar{f}_i, \forall i \in \mathcal{I}\}, \quad (10)$$

where B_i is the i -th row of matrix B and \bar{f}_i is the i -th entry of vector \bar{f} . It follows from (10) that if $\mathcal{I} = \{1, \dots, M\}$, then $\mathcal{F}(B, \bar{f}, \mathcal{I}) = \{x : Bx \leq \bar{f}\} = \mathcal{F}(B, \bar{f})$.

Definition 1 (Non-redundant/Redundant Index). Index $k \in \mathcal{I}$ is called *non-redundant* against set of indices \mathcal{I} if $\mathcal{F}(B, \bar{f}, \mathcal{I})$

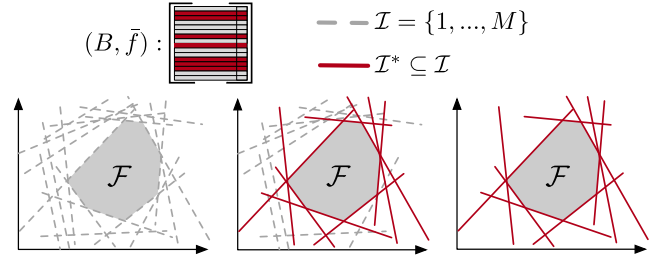


Fig. 1. Schematic representation of the equivalent description of a feasible region $\mathcal{F}(B, \bar{f}, \mathcal{I})$ by $\mathcal{F}(B, \bar{f}, \mathcal{I}^*)$ where $\mathcal{I} = \{1, \dots, M\}$ is the set of all indices of system (B, \bar{f}) and $\mathcal{I}^* \subseteq \mathcal{I}$ is the essential set of indices.

changes when index k is removed from \mathcal{I} :

$$k \in \mathcal{I} \text{ is non-redundant iff } \mathcal{F}(B, \bar{f}, \mathcal{I} \setminus \{k\}) \neq \mathcal{F}(B, \bar{f}, \mathcal{I}).$$

In analogy, index $k \in \mathcal{I}$ is called *redundant* if $\mathcal{F}(B, \bar{f}, \mathcal{I})$ does not change when k is removed from \mathcal{I} :

$$k \in \mathcal{I} \text{ is redundant iff } \mathcal{F}(B, \bar{f}, \mathcal{I} \setminus \{k\}) = \mathcal{F}(B, \bar{f}, \mathcal{I}).$$

Definition 2 (Essential Set/Index). A set of indices $\mathcal{I}^* \subseteq \{1, \dots, M\}$ is called *essential* to the system (B, \bar{f}) if it contains only non-redundant indices, i.e. no $k \in \mathcal{I}^*$ can be removed from \mathcal{I}^* without changing $\mathcal{F}(B, \bar{f}, \mathcal{I}^*)$ and $\mathcal{F}(B, \bar{f}, \mathcal{I}^*) = \{x : Bx \leq \bar{f}\}$. Accordingly, any index $k \in \mathcal{I}^*$ is called essential index.

Fig. 1 schematically illustrates a region $\mathcal{F}(B, \bar{f})$ defined by a redundant system (B, \bar{f}) and indicates the relation between essential and non-essential indices.

A. Efficient Essential Set Identification

To identify essential set \mathcal{I}^* , first we require a procedure that determines whether or not index k is redundant in $\mathcal{F}(B, \bar{f}, \mathcal{I})$. Following [23, Proposition 8.5], $k \in \mathcal{I}$ is non-redundant if and only if the LP

$$\text{LP-Test}(B, \bar{f}, \mathcal{I}, k): \quad p^* = \max_x B_k x \quad (11a)$$

$$\text{s.t.} \quad B_i x \leq \bar{f}_i \quad \forall i \in \mathcal{I} \setminus \{k\} \quad (11b)$$

$$B_k x \leq \bar{f}_k + 1 \quad (11c)$$

has an optimal solution x^* and the corresponding optimal value p^* is strictly greater than \bar{f}_k . Using the LP-Test as given in (11), it is possible to identify essential set \mathcal{I}^* by running LP-Test($B, \bar{f}, \mathcal{I}, k$) with $\mathcal{I} = \{1, \dots, M\}$ for all $k \in \mathcal{I}$. However, this requires solving a M -dimensional LP M times. This complexity can be significantly reduced by populating \mathcal{I} iteratively with identified essential indices, instead of always checking against complete set $\mathcal{I} = \{1, \dots, M\}$, [21], [23].

The resulting iterative process `RedundancyRemoval` is illustrated in Fig. 2. The procedure takes system (B, \bar{f}) and an interior point $z \in \mathcal{F}^\circ(B, \bar{f})$ as input and returns set \mathcal{I}^* of essential indices of system (B, \bar{f}) . If (B, \bar{f}) corresponds to the feasible region of the power flow problem, $z = 0$ is always an interior point of $\mathcal{F}(B, \bar{f})$, because zero nodal injections and, thus, zero-flows are always a solution to the power flow equations. The procedure is initialized with empty set $\mathcal{I} = \emptyset$, which is iteratively filled with essential indices, and the full set $\mathcal{J} = \{1, \dots, M\}$, which stores all indices that have to be checked. First, the procedure randomly selects an unchecked index k from \mathcal{J} and solves the LP-Test($B, \bar{f}, \mathcal{I} \cup \{k\}, k$), which returns p^* and x^* as per (11). If the LP-Test returns an

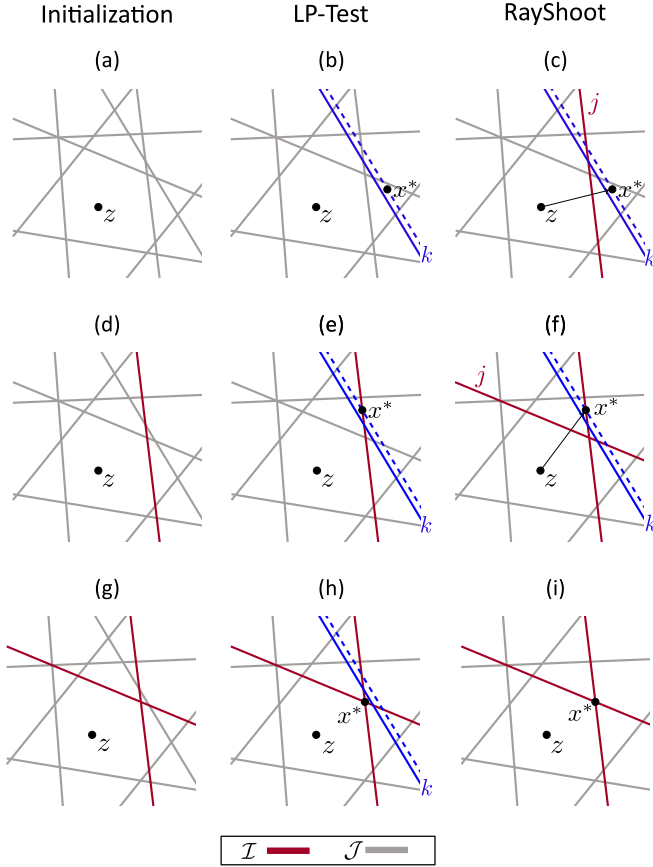


Fig. 2. Graphical (left) and algorithmic (right) itemization of essential set discovery procedure, where each row in the graphic corresponds to one iteration step of the algorithm and each column corresponds to one specific task that is performed in each iteration (as given by the column headers). Gray lines represent the constraints with indices to be checked, red lines represent the found essential constraints, blue solid lines represent the constraint that is checked in the current iteration and blue dashed lines represent the corresponding relaxed constraint $(\bar{f}_k + 1)$, see (11). (a) Initial state with $\mathcal{J} = \{1, \dots, M\}$, $\mathcal{I} = \emptyset$ and z some interior point; (b) Some index k is selected from \mathcal{J} and $\text{LP-Test}(B, \bar{f}, \mathcal{I}, k)$ is performed; (c) Because \mathcal{I} is empty in the initial iteration k is always non-redundant against \mathcal{I} and the most restricting constraint j in the direction of $(x^* - z)$ is added to \mathcal{I} ; (d) The next iteration starts with \mathcal{I} now containing one essential index; (e) Because k was non-redundant in the last step, it remains selected and $\text{LP-Test}(B, \bar{f}, \mathcal{I}, k)$ is performed; (f) Now, k is again non-redundant against \mathcal{I} and the most restricting constraint j in the direction of $(x^* - z)$ is added to \mathcal{I} ; (g) The next iteration starts with \mathcal{I} now containing two essential indices; (h) Because k was non-redundant in the last step, it remains selected and $\text{LP-Test}(B, \bar{f}, \mathcal{I}, k)$ is performed; (i) Index k is now redundant against set \mathcal{I} and is therefore removed from set \mathcal{J} ; The procedure repeats until all elements have been removed from \mathcal{J} .

optimal solution and $p^* > \bar{f}_k$, then \mathcal{I} does not yet contain the index of a constraint that restricts $\mathcal{F}(B, \bar{f}, \mathcal{I})$ in the direction of $x^* - z$, see Fig. 2b). However, because set \mathcal{I} is initialized empty, indices can be non-redundant against \mathcal{I} but not essential to (B, \bar{f}) . In other words, there might exist a constraint with index j in the direction of $x^* - z$ that is more restrictive than the constraint with index k . As shown in Fig. 2c), the auxiliary procedure RayShoot identifies the most restrictive constraint in the direction of $x^* - z$ by shooting a ray from z in the direction of $x^* - z$ and returning index j of the first hyperplane $\{x : B_j x = \bar{f}_j\}$ that it crosses. See Appendix C for a detailed description of RayShoot . This index j is guaranteed to be an essential index of (B, \bar{f}) . Thus, j is added to \mathcal{I} and removed from \mathcal{J} . Note that if $j \neq k$, then k remains in \mathcal{J} to be checked again, see Fig. 2e). If $\text{LP-Test}(B, \bar{f}, \mathcal{I} \cup \{k\}, k)$ determines k to be redundant against \mathcal{I} , see Fig. 2h), then k is guaranteed to be not essential because \mathcal{I} only contains essential indices. In this case, no new essential index has been found and k is removed from \mathcal{J} , see Fig. 2i). The process is repeated until \mathcal{J} is empty. The resulting set \mathcal{I} contains all essential indices and therefore $\mathcal{I} = \mathcal{I}^*$. This essential set \mathcal{I}^* is a minimal

Algorithm 1: $\text{RedundancyRemoval}(B, \bar{f}, z)$

input : System of inequalities given by B and \bar{f} ,
Interior point z
output: Returns the set \mathcal{I} of non-redundant inequality indices of the system $Bx \leq \bar{f}$

begin
 $\mathcal{I} \leftarrow \emptyset$; // Set of essential indices
 $\mathcal{J} \leftarrow \{1, \dots, M\}$; // Indices to check
while $|\mathcal{J}| > 0$ **do**
 select an index k from \mathcal{J} ;
 $(p^*, x^*) \leftarrow \text{solve LP-Test}(B, \bar{f}, \mathcal{I} \cup \{k\}, k)$;
 if $\exists x^*$ **and** $p^* > \bar{f}_k$ **then**
 $\alpha \leftarrow \text{true}$;
 $j \leftarrow \text{RayShoot}(B, \bar{f}, z, x^*)$;
 // Returns an essential index
 else
 $\alpha \leftarrow \text{false}$;
 end
 if α **then**
 $\mathcal{I} \leftarrow \mathcal{I} \cup \{j\}$; // Update essential
 $\mathcal{J} \leftarrow \mathcal{J} \setminus \{j\}$; // Remove checked
 else
 $\mathcal{J} \leftarrow \mathcal{J} \setminus \{k\}$; // Remove checked
 end
end
return \mathcal{I}
end

representation of the contingency feasible region, see (7), and each essential index represents a specific critical line under a specific outage and therefore can be denoted as a minimal set of CBCOs.

While the complexity of the RedundancyRemoval remains dominated by the LP-Test, it is now performed M times with at most $|\mathcal{I}^*|$ constraints. The worst-case performance of the RedundancyRemoval occurs when all essential indices are immediately found in the first $|\mathcal{I}^*|$ iterations. Then, LP-Test is performed $|\mathcal{I}^*|$ times with less than $|\mathcal{I}^*|$ constraints and $M - |\mathcal{I}^*|$ times with $|\mathcal{I}^*|$ constraints. The RayShoot procedure performs basic vector calculations in the $\mathbb{R}^{M \times N}$ space and is performed $|\mathcal{I}^*|$ times. Its complexity is therefore linear against MN and dominated by the complexity of LP-Test.

Remark 2. The capacity of a line is independent from the direction of the flow, thus the load flow constraints are identical for the upper and lower bound and an essential set for the upper bound corresponds to an essential set for the lower bound. Thus, it is sufficient to perform the RedundancyRemoval only on the positive PTFD matrices to speed-up the essential

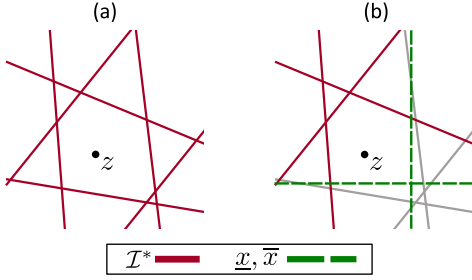


Fig. 3. Illustration of two essential sets \mathcal{I}^* with and without considerations for bounds on x : a) $\mathcal{F}(B, \bar{f}, \mathcal{I}^*) = \{x : Bx \leq \bar{f}\}$ b) $\mathcal{F}(B, \bar{f}, \mathcal{I}^*|_{(\underline{x}, \bar{x})}) = \{\underline{x} \leq x \leq \bar{x} : Bx \leq \bar{f}\}$

set identification.

B. Conditional Redundancy

The essential set identification as presented in previous Section III-A only depends on redundancies that are inherent to system (B, \bar{f}) , i.e. that are given by the power flow limits and contingency scenarios as in (7)–(9). Thus, resulting essential set \mathcal{I}^* contains all non-redundant indices assuming that x is unbounded. While it is useful to find such a general essential set, practical application usually includes specific generation units, demand- and renewable time-series along with the grid infrastructure. This allows to determine upper and lower bounds for nodal injections x_t . Considering bounds on x_t in the proposed algorithm, can render certain essential indices unnecessary, because the specific allocation of nodal injections to overload certain CBCOs will never occur given the known technical limits. In other words, we can find a set $\mathcal{I}^*|_{(\underline{x}, \bar{x})} \subseteq \mathcal{I}^*$ by bounding x_t as schematically illustrated in Fig. 3. Resulting set $\mathcal{I}^*|_{(\underline{x}, \bar{x})}$ is then sufficient to define $\mathcal{F}(B, \bar{f})$ under the condition that x is bounded by (\underline{x}, \bar{x}) :

$$\begin{aligned} \mathcal{F}(B, \bar{f}, \mathcal{I}^*) &= \mathcal{F}(B, \bar{f}, \mathcal{I}^*|_{(\underline{x}, \bar{x})}) \\ &= \{\underline{x} \leq x \leq \bar{x} : Bx \leq \bar{f}\}. \end{aligned} \quad (12)$$

Bounds (\underline{x}, \bar{x}) strictly relate to the parameters and available data of the modeled system. In typical applications, the modeled system remains static over \mathcal{T} , so that implicit bounds on nodal injections will always hold and a smaller essential set will provide a reduction of model complexity without compromising the validity of the resulting SCOPF. First, we compute asymmetrical bounds by determining the maximum positive and negative nodal injections:

$$\tilde{x}_i = \min(d_{t,i}, t \in \mathcal{T}) + \min(M_i \underline{g}_t, t \in \mathcal{T}) \quad (13)$$

$$\hat{x}_i = \max(M_i \bar{g}_t, t \in \mathcal{T}), \quad (14)$$

where \tilde{x}_i and \hat{x}_n are the maximum negative and maximum positive nodal injection at n given the available demand and generation parameters. Note that these bounds can be extended to accommodate renewable in-feed time series or storage capacities. However, as indicated in Remark 2, feasible region $\mathcal{F}(B, \bar{f})$ is symmetric. Thus, bounds on x have to be included symmetrically and we define:

$$-\underline{x} = \bar{x} = \max(|\tilde{x}|, |\hat{x}|). \quad (15)$$

Using these bound to compute $\mathcal{I}^*|_{(\underline{x}, \bar{x})}$ will further reduce the resulting problem size of the SCOPF (9).

IV. IMPACT SCREENING

The run-time of the `RedundancyRemoval` is directly related to the initial number of constraints M since each index $k \in \{1, \dots, M\}$ has to be checked. It is therefore desirable to reduce the number of constraints beforehand if possible. As described in Section II-B, contingencies are considered by computing how line flows are distributed across all other lines in the case of an outage. Each line is only significantly affected by an outage of its physical neighbors in close proximity, while a large number of contingencies in greater electrical distance have hardly any effect on its post-contingency power flow.

Consider the outage of a line $o \in \mathcal{L}$. As per (3), LODF_{l_o} determines how the pre-contingency power flow of line o is distributed among all other lines $l \neq o, l \in \mathcal{L}$. Because the power flow on any line is bounded by \bar{f} , the impact any line outage can have on any other line is bounded by the respective LODF multiplied with the maximum flow on this line:

$$|f_{t,l}^o - f_{t,l}^0| = |\text{LODF}_{l_o} f_{t,o}^0| \leq |\text{LODF}_{l_o} \bar{f}_o|. \quad (16)$$

By reserving a small capacity margin η on each line, every outage that impacts this line by less than η can be disregarded. In other words, all rows PTDF_l^o can be omitted if

$$\frac{\text{LODF}_{l_o} \bar{f}_o}{\bar{f}_l} < \eta. \quad (17)$$

effectively reducing the length of the input matrix B and therefore reducing the run-time of the `RedundancyRemoval`.

Depending on the implementation, chosen threshold η either reflects a safety margin by reducing the available line capacity $(1 - \eta)\bar{f}_l$ or an allowable *worst-case* short-term overload by virtually increasing the line capacity $(1 + \eta)\bar{f}_l$. Both approaches, are typically used in practice to accommodate parameter uncertainty, [24]. Note that this approach alters the result of the SCOPF by creating an either slightly larger or slightly smaller feasible region. This inaccuracy has to be analysed and weighed against the benefit of the increased run-time of the `RedundancyRemoval` for the specific problem at hand.

V. CASE STUDY

We investigate the performance of the presented procedures by running two numerical case studies. The first data-set is the IEEE 118-bus system with 186 lines and line capacity information taken from [25]. We consider all N-1 outage scenarios that that the resulting number of constraints in the SCOPF is 66,216. This case provides a comprehensive summary of the mechanics of the proposed constraint reduction process. Second we use a larger 453-node data set of the German transmission system (DE case) to showcase the performance for common real-world multi-period applications. The DE case comprises almost 2 million constraints related to its 995 lines. Table I summarizes both cases.

We show four stages of constraint reduction that have been used to solve the N-1 SCOPF. Stage “Full” considers all combinations of branches and outages in the positive halfspace, i.e. no explicit constraint reduction has been applied beyond ignoring the symmetry of the flow limits as discussed in Remark 2. The “Pre” (preprocessed) stage includes the impact screening as described in Section IV. The stages “RR” and

TABLE I
OVERVIEW: CASE STUDIES

	Nodes	Lines	Generators	N-1 Flow Constraints
IEEE 118	118	186	116	66,2160
DE	453	995	4226	1,934,280

“CRR” apply the `RedundancyRemoval` procedure without and with conditional redundancies, see Section III-B. Note that those stages are presented here to itemize the effect of the different parts of the reduction algorithm. For actual application of the proposed method there is only one stage to use, i.e. “CRR”. All results are compared in terms of the resulting number of constraints and the corresponding time to solve the optimal power flow model (6) using these constraints.

The computations have been performed on a standard PC workstation with an Intel 8th generation i5 processor and 16GB memory. The optimal power flow model and the reduction procedures have been implemented in the open source *Power Market Tool* (POMATO, [22]). The tool is written in Python for data pre- and postprocessing and uses the Julia/JuMP package, [26], in combination with the Gurobi solver, [27], as its optimization kernel. To allow direct comparison, dual simplex was used and the presented times are the times reported by the solver, including presolve.

A. IEEE 118-bus Case

Table II itemizes the number of constraints, the respective solvetimes and objective values for all constraint reduction stages in the IEEE 118-bus case. The OPF has been solved for a single time step. For the preprocessing phase, the impact screening margin set to $\eta = 5\%$ which reduces the set of constraints by 87% to 4,152 and thus reducing the solvetime by 81%. The small increase in the objective value (ca. 3%) is explained by the implicit line capacity reduction of the impact screening margin, see Section V-C.

Running `RedundancyRemoval` further reduces this set by 41% to 2,465 and including conditional redundancy, as described in Section III-B, yields a set of only 518 CBCOs, that guarantee a N-1 SCOPF. Thus, instead of L relevant contingencies for L lines we observe an average of 2.78 critical outages per line. This represents a total removal of over 98% of the constraints and results in a 97% reduction of the time needed to solve the problem. Furthermore, we observe that the objective value remains unchanged after the impact screening. This verifies, that the reduction due to Algorithm 1 indeed only removes redundant constraints. The process time of `RedundancyRemoval` for the 118-bus case is around 7min without and below 1min with conditional redundancy. This demonstrates, that the presented algorithm is more efficient the more redundant the system is, i.e. the fewer non-redundant constraints can be found. Note that the reported process time refers to the runtime of the `RedundancyRemoval`.

B. DE Case

The DE case solves a multi-period nodal market clearing for the German power system including inter-temporal constraints for energy storages. The power plant data is based on [28] and the spacial distribution and grid topology is based on

TABLE II
IEEE 118-BUS CASE CONSTRAINT AND SOLVETIME REDUCTION

	Full	Pre	RR	CRR
# Constraints	33,108	4,152	2,465	518
Process Time [s]			396	64.9
Presolve [s]	3.84	0.45	0.27	0.07
Solvetime [s]	7.13	1.34	0.76	0.23
Objective	119,996	124,103	124,103	124,103
total constraint reduction:		87%	93%	98%
additional constraint reduction:		87%	41%	79%
total solvetime reduction:		81%	89%	97%
additional solvetime reduction:		81%	43%	70%

TABLE III
DE CASE CONSTRAINT REDUCTION

	Full	Pre	RR	CRR
# Constraints	967,140	14,523	10,695	2,629
Process Time [s]			136,495	11,719
total constraint reduction		98.5%	98.9%	99.7%
additional constraint reduction		98.5%	26%	75%

[29]. The large set of power plants is due to a detailed regionalization of small scale, decentralized power plants. This case represents a real world application with a prohibitively large linear problem. Indeed, the the full set of constraints cannot be solved by the computer hardware used for this case study as the system runs out of memory before an optimal solution has been obtained. While approaching the problem with more powerful hardware might be able to overcome this, the application of the proposed redundancy removal procedures makes this problem solvable. Table III shows that the “CRR” method removes 99.7% of all constraints within 195min processing time. The resulting average number of critical outages per line is 2.64 which is surprisingly similar to the 118-bus case. Preprocessing alone reduces the number of constraints already by over 98% with a impact screening margin of $\eta = 5\%$. An additional 26%, 75% are achieved by the `RedundancyRemoval` without and with conditional redundancy, respectively. Again, the processing time of the `RedundancyRemoval` itself is larger in the “RR” stage relative to “CRR” as the problem is less redundant.

The resulting set of CBCOs is used to solve a N-1 SCOPF for two time series of 10 and 24 time steps. The solvetimes and objective values are itemized in Tables IV and V. As there is no data for the “Full” stage, the time reductions are reported relative to the “Pre” stage. While the problem was not solvable with the full set of constraints, after “CRR” reduction an optimal solution was found within 13.5s for the 10-time step run and 22.87s for the 24-time step run. Compared to the 10-time step run, the 24-time step run shows a higher total time reduction both absolute as well as relative to the constraint reduction. This highlights the positive effect of the larger time series, where the benefits of the constraint reduction apply in every time step. All stages in the two runs result in exactly the same objective value verifying the the removal of only redundant constraints.

C. Impact Screening

As described in Section IV, the impact screening implicitly reduces the available line capacity in favor of disregarding

TABLE IV
DE CASE SOLVETIME REDUCTION (RELATIVE TO PRE) FOR 10 TIME STEPS

	Full	Pre	RR	CRR
Presolve [s]	NA	93.4	84.41	13.5
Solvetime [s]	NA	283.19	250.29	44.82
Objective	NA	2,993,021	2,993,021	2,993,021
total solvetime reduction:			12%	84%
additional solvetime reduction:			12%	82%

TABLE V
DE CASE SOLVETIME REDUCTION (RELATIVE TO PRE) FOR 24 TIME STEPS

	Full	Pre	RR	CRR
Presolve [s]	NA	507.7	220.53	22.87
Solvetime [s]	NA	1,707.56	714.37	89.53
Objective	NA	8,764,696	8,764,696	8,764,696
total solvetime reduction:			58%	95%
additional solvetime reduction:			58%	87%

outages which can not exceed this margin in case of an outage. While this significantly reduces the number of considered contingencies, the available transfer capacity of the network is reduced. The reduced network capacity correlates with a higher objective value as cheaper generators are more restricted to supply electrically distant nodes. To itemize the effect of the choice of the margin η , the DE case 10-time step run was repeated with different settings for η . Fig. 4 shows the resulting number of CBCOs and objective values in the optimal solution. The effect of η on the objective is closely linear and we observe that an increase in η of 1% translates into a mild increase of the objective value of ca. 0.5%. On the other hand, the resulting amount of CBCOs is reduced drastically already by small values of η . Those results highlight how every outage in a meshed grid only has a certain reach and that the number of outages relevant for a specific branch is spatially restricted. Fig. 5 shows this effect by color-coding the relative outage sensitivity of all lines in the network towards the highlighted blue line. By showing all lines with an impact of less than 1% in gray, we see that mostly neighboring and parallel lines in close proximity have a significant impact on the highlighted line.

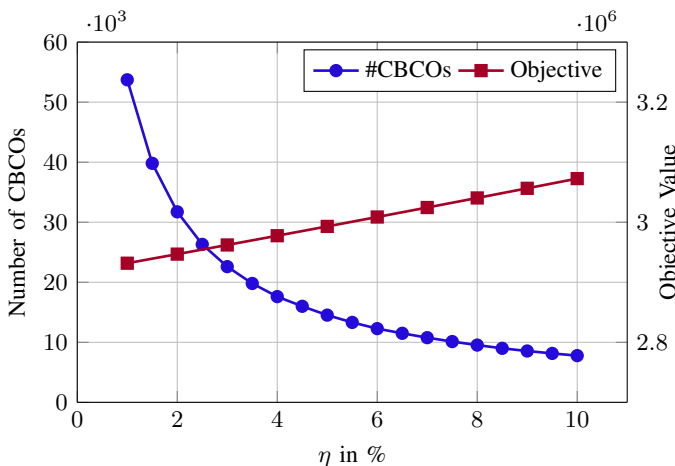


Fig. 4. Effect of impact screening margin η on the resulting number of CBCOs for the DE 10-time step case.

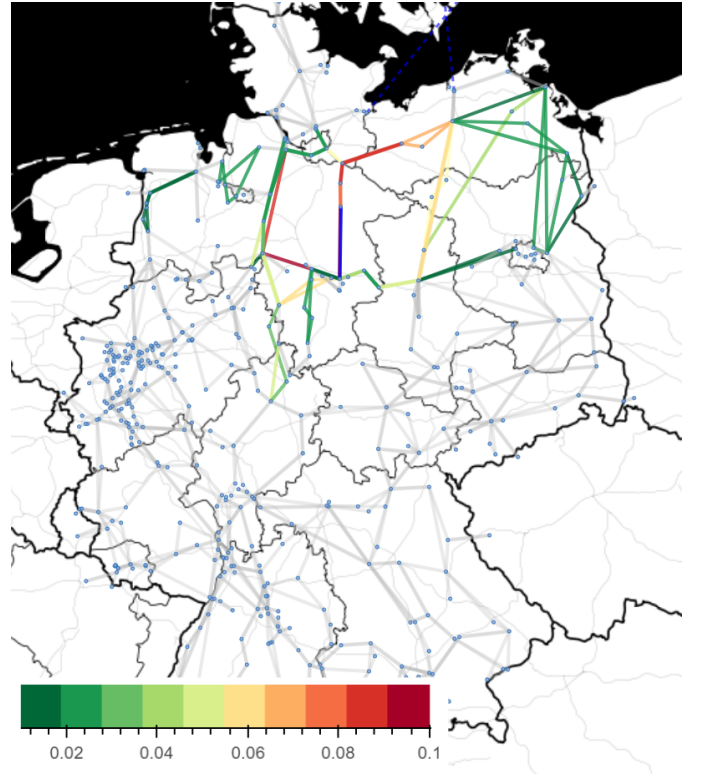


Fig. 5. Impact of outages towards the highlighted (blue) line; Grey lines indicate a sensitivity of less than 1%.

VI. CONCLUSION

This paper proposed an efficient and scalable algorithm to find the minimal set of constraints for fast solution of security constrained optimal power flow. The constraint reduction comes with solvetime benefits that increase with longer time series. The redundancy removal is computationally tractable and additionally impact screening allows to filter specific line outages without compromising security of operation to reduce the runtime of the essential set identification. The necessary margins for bounds and sensitivity of impact screening can be easily attributed to margins used in practice. Further, we showed that conditional redundancy improve constraint reduction as well as process time and should be the preferred configuration of usage. In case of line outages, the identified essential constraints represents the set of critical branches under critical outages. The proposed methods qualify to be used in a broad variety of applications in techno-economic studies that rely on an accurate and security constrained network representation, e.g. studies on redispatch or flow based market coupling.

REFERENCES

- [1] ENTSO-E, "Power Facts Europe 2019," 2019. [Online]. Available: docstore.entsoe.eu
- [2] K. Van den Bergh, J. Boury, and E. Delarue, "The flow-based market coupling in central western europe: Concepts and definitions," *The Electricity Journal*, vol. 29, no. 1, pp. 24–29, 2016.
- [3] Amprion, "Flow based market coupling: Development of the market and grid situation 2015-2017," 2018. [Online]. Available: www.amprion.net
- [4] F. Capitanescu *et al.*, "State-of-the-art, challenges, and future trends in security constrained optimal power flow," *Electric Power Systems Research*, vol. 81, no. 8, pp. 1731–1741, 2011.
- [5] F. U. Leuthold, H. Weigt, and C. von Hirschhausen, "A large-scale spatial optimization model of the european electricity market," *Networks and spatial economics*, vol. 12, no. 1, pp. 75–107, 2012.

- [6] A. J. Wood and B. F. Wollenberg, *Power generation, operation, and control*. John Wiley & Sons, 1996.
- [7] B. Stott and E. Hobson, "Power system security control calculations using linear programming, Part I & II," *IEEE Trans. Power App. Syst.*, no. 5, pp. 1713–1720, 1978.
- [8] V. Brandwajn, "Efficient bounding method for linear contingency analysis," *IEEE Trans. Power Syst.*, vol. 3, no. 1, pp. 38–43, 1988.
- [9] F. Capitanescu *et al.*, "Contingency filtering techniques for preventive security-constrained optimal power flow," *IEEE Trans. Power Syst.*, vol. 22, no. 4, pp. 1690–1697, 2007.
- [10] F. Capitanescu and L. Wehenkel, "A new iterative approach to the corrective security-constrained optimal power flow problem," *IEEE Trans. Power Syst.*, vol. 23, no. 4, pp. 1533–1541, 2008.
- [11] S. Fliscounakis *et al.*, "Contingency ranking with respect to overloads in very large power systems taking into account uncertainty, preventive, and corrective actions," *IEEE Trans. Power Syst.*, vol. 28, no. 4, pp. 4909–4917, 2013.
- [12] Y. Fu, Z. Li, and L. Wu, "Modeling and solution of the large-scale security-constrained unit commitment," *IEEE Trans. Power Syst.*, vol. 28, no. 4, pp. 3524–3533, 2013.
- [13] R. Fischl, G. Ejebe, and J. DeMaio, "Identification of power system steady-state security regions under load uncertainty," in *IEEE Power App. Syst.*, vol. 95, no. 6. IEEE, 1976, pp. 1767–1767.
- [14] A. J. Ardakani and F. Bouffard, "Identification of umbrella constraints in dc-based security-constrained optimal power flow," *IEEE Transactions on Power Systems*, vol. 28, no. 4, pp. 3924–3934, 2013.
- [15] B. Hua *et al.*, "Eliminating redundant line flow constraints in composite system reliability evaluation," *IEEE Trans. Power Syst.*, vol. 28, no. 3, pp. 3490–3498, 2013.
- [16] L. Roald and D. K. Molzahn, "Implied constraint satisfaction in power system optimization: The impacts of load variations," *arXiv preprint arXiv:1904.01757*, 2019.
- [17] R. Madani, J. Lavaei, and R. Baldick, "Constraint screening for security analysis of power networks," *IEEE Trans. Power Syst.*, vol. 32, no. 3, pp. 1828–1838, 2016.
- [18] Q. Zhai *et al.*, "Fast identification of inactive security constraints in sec problems," *IEEE Trans. Power Syst.*, vol. 25, no. 4, pp. 1946–1954, 2010.
- [19] A. J. Ardakani and F. Bouffard, "Acceleration of umbrella constraint discovery in generation scheduling problems," *IEEE Trans. Power Syst.*, vol. 30, no. 4, pp. 2100–2109, 2014.
- [20] —, "Prediction of umbrella constraints," in *2018 Power Systems Computation Conference (PSCC)*. IEEE, 2018, pp. 1–7.
- [21] K. L. Clarkson, "More output-sensitive geometric algorithms," in *Ann. Symp. on Foundations of Comp. Science*. IEEE, 1994, pp. 695–702.
- [22] R. Weinhold and R. Mieth. (2019) Power Market Tool - POMATO. [Online]. Available: <https://github.com/korpuskel91/pomato>
- [23] K. Fukuda, "Lecture: Polyhedral computation, spring 2016," *Institute for Operations Research and Institute of Theoretical Computer Science. ETH Zurich*. Available online at www.inf.ethz.ch, 2016.
- [24] D. Bienstock, *Electrical Transmission System Cascades and Vulnerability: An Operations Research Viewpoint*. SIAM, 2016, vol. 22.
- [25] R. D. Christie, "IEEE PES Power Grid Library - Optimal Power Flow - v19.01," github.com/power-grid-lib, 2019.
- [26] I. Dunning, J. Huchette, and M. Lubin, "Jump: A modeling language for math. optimization," *SIAM Review*, vol. 59, no. 2, pp. 295–320, 2017.
- [27] Gurobi Optimization, LLC, "Gurobi optimizer reference manual," 2018. [Online]. Available: <http://www.gurobi.com>
- [28] Open Power System Data. (2018) Power plants database. [Online]. Available: data.open-power-system-data.org
- [29] F. Kunz *et al.*, "Electricity, Heat and Gas Sector Data for Modelling the German System," DIW Berlin, Tech. Rep. 92, 2017. [Online]. Available: www.diw.de
- [30] Jiachun Guo *et al.*, "Direct calculation of line outage distribution factors," *IEEE Trans. Power Sys.*, vol. 24, no. 3, pp. 1633–1634, 2009.

APPENDIX

A. PTDF Derivation

Assuming that voltage magnitudes are fixed, phase angle differences between neighbouring nodes are small and reactance dominates resistance on all lines, the active power flow on line l from node s to node r can be written in terms of the phase angle difference between those nodes such that

$$f_{t,l} = (x_{t,l})^{-1}(\theta_{t,s} - \theta_{t,r}), \quad (\text{A.1})$$

where $\theta_{t,n}$ is the voltage angle at node n at time t and we define θ_t to collect all $\theta_{t,n}$, $n \in \mathcal{N}$. All nodal injections and power flows are balanced such that:

$$x_{t,n} = \sum_{\mathcal{L}_n} f_{t,l}, \quad (\text{A.2})$$

where \mathcal{L}_n is the set of lines connected to node n . Defining incidence matrix $A \in \{-1, 0, 1\}^{L \times N}$ such that all entries are zero except $A_{(l,n)} = 1$ if node n is the sending node of line l and $A_{(l,n)} = -1$ if n is the receiving node of line l (A.1) and (A.2) can be written in their vector forms as

$$f_t = X^{-1}A\theta_t = B^{(f)}\theta_t, \quad (\text{A.3})$$

$$x_t = A^\top X^{-1}A\theta_t = B^{(n)}\theta_t, \quad (\text{A.4})$$

where diagonal matrix $X \in \mathbb{F}^{L \times L}$ collects line reactances such that $X_{(l,l)} = b_l, \forall l \in \mathcal{L}$ and $B^{(f)} \in \mathbb{R}^{L \times N}$, $B^{(n)} \in \mathbb{R}^{N \times N}$ is the line and bus susceptance matrix, respectively. Next, because (A.1) is based on angle differences, we define a reference (slack) node with fixed phase angle. Without loss of generality we choose the index of the slack node to be $n_{\text{slack}} = 1$. Then $B^0 \in \mathbb{R}^{L \times N}$ is defined by:

$$B^0 = B^{(f)} \begin{bmatrix} 0 & 0 \\ 0 & (\tilde{B}^{(n)})^{-1} \end{bmatrix} \quad (\text{A.5})$$

where $\tilde{B}^{(n)} \in \mathbb{S}^{N-1}$ is the bus susceptance matrix without the row and column associated with the slack bus (first row and first column in our case).

B. LODF derivation

Given outage scenario $c \subseteq \mathcal{L}$ $\text{LODF} \in \mathbb{R}^{L \times L}$ can be calculated as shown in [30]:

$$\text{LODF}_c = B_c^0(I - B_{c,c}^0)^{-1} \quad (\text{B.1a})$$

where $B_{c,c}^0$ is the $|c| \times |c|$ matrix collecting the rows and columns of B^0 corresponding to the outages in c and I is the identity matrix of fitting dimensions.

C. Implementation of RayShoot

Algorithm 2: RayShoot(B, \bar{f}, z, x^*)

input : System (B, \bar{f})

Interior point z

Point on or outside of feasible region x^*

output: Index of first inequality that limits a ray starting at z in the direction of r

begin

$\mathcal{H} \leftarrow \emptyset$; // Set of crossed hyperplanes

$\epsilon \leftarrow \epsilon^{\text{init}}$; // Set initial ray increment

$r = \frac{x^* - z}{\|x^* - z\|_2}$; // Set direction of ray

while $|\mathcal{H}| \neq 1$ **do**

$z \leftarrow z + \epsilon r$; // Add increment to ray

$\mathcal{H} \leftarrow \{i \mid B_i z > \bar{f}_i\}$;

if $|\mathcal{V}| > 1$ **then**

$z \leftarrow z - \epsilon r$; // Go back one step

$\epsilon \leftarrow \epsilon/10$; // Reduce step size

end

end

return \mathcal{H}

end
